Modeling Method and Experimental Study on the Random Distribution of Abrasive Particles in the Jet Cutting Process

Long Feng
Shandong University of Science and Technology
Qiang Zhang
Shandong University of Science and Technology
MingChao Du (13156394970@163.com)
Shandong University of Science and Technology
Chunyong Fan
Shandong University of Science and Technology
Kun Zhang
Shandong University of Science and Technology

Research Article

Keywords: abrasive waterjet cutting, random algorithm, SPH algorithm, cutting profile

Posted Date: September 7th, 2021

DOI: https://doi.org/10.21203/rs.3.rs-870164/v1

Modeling method and experimental study on the random distribution of abrasive particles in the jet cutting process

Long Feng, Qiang Zhang, Mingchao Du*, Chunyong Fan, Kun Zhang

College of mechanical and Electronic Engineering, Shandong University of Science and Technology, Qingdao 266590, China

Long Feng:

Email: fenglong126224@126.com Fax: + 86532-86057540

Telephone number: +8613964813381

Qiang Zhang:

Email: 415564476@qq.com Fax: + 86532-86057540

Mingchao Du:

Email: 13156394970@163.com Fax: + 86532-86983300

Telephone number: +8613156394970

Chunyong Fan:

Email: 1414642950@qq.com Fax: +86532-86057540

Telephone number: +8618266632167

Kun Zhang:

Email: zhangkunliaoning@163.com Fax:

Telephone number: +8615041800261

Abstract: The distribution of abrasive particles in fluids is an important research topic in the study of abrasive waterjet cutting processes. However, it is impossible to obtain the accurate distribution law and influencing factors by performing only experiments; therefore, it is necessary to study abrasive waterjet cutting processes with the help of numerical models. The existing numerical models usually adopt the form of artificial settings for the distribution of abrasive particles in fluid. This method cannot accurately simulate the random distribution of particles. In this paper, the random algorithm method is used to simulate the impact azimuth and the random distribution of abrasive particles in water. The smoothed particle hydrodynamics (SPH) method is used to simulate the distribution of abrasive particles and the process of jet impingement. The influence of the particle distribution on the simulation results is studied. Comparisons show that the dent formed by the jet impinging on the target with random abrasive particles is similar to the dent from the actual cut, and the contour distribution of the dent is more uniform than that of the cut. The simulation results obtained by the SPH method are accurate.
Keywords: abrasive waterjet cutting; random algorithm; SPH algorithm; cutting profile

1. Introduction

An abrasive waterjet is a solid-liquid two-phase medium jet formed by mixing abrasive particles and high-speed water. The main difference between the abrasive waterjet and pure waterjet is that the cutting pressure of the abrasive waterjet is less than that of the pure waterjet, but the cutting efficiency is improved, and there is no thermal reaction or chemical reaction during the cutting process. This technology is widely used in the fields of oil exploitation, mechanical processing, mining and tunnel excavation. The influence of abrasive particles is the most critical and complex factor affecting the abrasive waterjet cutting process. Clarifying the distribution and movement of particles in water is of great importance for understanding the cutting process. M. S. eltoby [1] established a finite element analysis model of a micro abrasive erosion material, and the model was solved to simulate the erosion process of multiple particles. However, during modeling, the abrasive geometry was simplified to a spherical shape, and the sharp edges of the abrasive particles were ignored. Babets et al. [2] used the volume of fluid (VOF) model to take the fluid medium as the continuous phase and the abrasive particles as the dispersed phase, and the Lagrangian method was used to track the particles to obtain the variation rules of parameters such as the velocity, turbulent kinetic energy, density and particle trajectory. Ahmed et al. [3] considered both abrasive particles and water to be continuous phases while analyzing them using the Euler method, and determined the optimal incident angle of abrasive particles. Feng[4] used the SPH method to numerically model the abrasive waterjet cutting process. In the model, abrasive particles were parameterized and expressed in the form of SPH particles. The model can simulate the movement and impact of particles in water. Liang et al. [5] established a multiphase flow model to quantitatively describe the flow characteristics of abrasive waterjets, clarify the actual performance of abrasive waterjets in the contact area, and establish a new fuzzy prediction system to predict the turbulence characteristics according to the processing parameters. Dong et al. [6] established a model of the impact of angular particles on different forms of materials

and solved it with the SPH method. The impact morphology of different forms of angular particles was simulated, but the influencing factors of the water jet were not considered.

The following limitations exist in the research of abrasive waterjet cutting processes: a) The influence of an abrasive particle shape is ignored in some models, so the effect of abrasive particles on the cutting performance cannot be studied. b) The geometric modeling of abrasive particles is more difficult in conventional SPH numerical modeling than other modeling approaches, so the average density method of the SPH method is often used to simulate the impact process of abrasive waterjets. c) Waterjet and abrasive particles are modeled separately, without considering the influence of coupling factors.

Based on the reasons described above, the SPH algorithm is used to parameterize the model of abrasive particles, the random algorithm is introduced to simulate the random distribution of particles in fluid, and the influence of the particle distribution on the calculation model in the modeling process is studied. In this paper, when modeling the abrasive waterjet cutting process, the combination of the SPH modeling method and random algorithm can not only highlight the advantages of the SPH method in determining the impact but also improve the simulation of the abrasive particle distribution state and improve the accuracy of the simulation. The other sections of this paper are summarized as follows. In the second section, the basic principle of SPH and the SPH modeling method of the abrasive waterjet cutting model are introduced. In the third section, random algorithm modeling of abrasive particles is carried out, and the numerical simulation results without the random algorithm and with the random algorithm are compared and analyzed. In the fourth section, the abrasive waterjet cutting process is experimentally studied, and the simulation results are compared with the experimental data to verify the effectiveness and accuracy of the simulation method. The fifth part summarizes the research conclusion.

2. Basic theory of the SPH algorithm and modeling process of abrasive water jets

2.1 Basic theory of the SPH method

The basic principles of SPH can be summarized as follows[7]: a) First, the SPH algorithm is a meshless algorithm that uses a series of arbitrarily distributed particles instead of meshing when describing the problem domain. b) In the SPH algorithm, the field function needs to be approximately solved, and the integral representation method is used during this process, which has the advantage of improving the stability of the solution because the integral method has a smooth effect and is equivalent to the weak form equation. The above process, called kernel approximation, is the first step in the construction of the SPH equation. c) The second key step is called particle approximation. To replace the integral expression of the field function and its derivatives, the corresponding values of the neighboring particles in a certain region are added and summed. This process can produce a discrete system matrix, which can effectively improve the calculation efficiency. d) The SPH algorithm is adaptive. Particle approximation is needed during every calculation step, and the particles in the process of particle approximation are the particles distributed in the current computational domain. e) The Lagrangian characteristics of the SPH algorithm applies

the particle approximation method to the field function correlation terms so that only the discretized ordinary differential equations related to time can be obtained. f) The dynamic properties of the SPH algorithm are obtained using the display integral to calculate the ordinary differential equations, and the fastest time integration can be obtained. At the same time, the change in the field variables of all the particles with time can be obtained.

Kernel approximation process[8]:

In the SPH method, the integral representation of function *f*(x) is shown in equation (1),

$$f(\boldsymbol{x}) = \int_{\Omega} f(\boldsymbol{x}')\delta(\boldsymbol{x} - \boldsymbol{x}')\mathrm{d}\boldsymbol{x}' \tag{1}$$

where *f* is a function of *x*, Ω is the integral volume of *x*, and $\delta(x - x')$ is the Dirac function.

The process of replacing the Dirac function with the smooth function W (*x*-*x* ', *H*) is called the kernel approximation. Therefore, equation (1) can be written as follows,

$$f(\boldsymbol{x}) \approx \int_{\Omega} f(\boldsymbol{x}')W(\boldsymbol{x} - \boldsymbol{x}', h)\mathrm{d}\boldsymbol{x}' \tag{2}$$

where the support domain and problem domain of smooth function *W* should satisfy the following conditions:

a) The normalized condition is shown in equation (3),

$$\int_{\Omega} W(\boldsymbol{x} - \boldsymbol{x}', h)\mathrm{d}\boldsymbol{x}' = 1 \tag{3}$$

b) When the value of smooth length h tends to 0, the smooth function is approximately equal to the Dirac function,

$$\lim_{\mathrm{h}\to 0} W(\boldsymbol{x} - \boldsymbol{x}', h) = \delta(\boldsymbol{x} - \boldsymbol{x}') \tag{4}$$

c) For the compact support condition, the following equation can be obtained when$|\boldsymbol{x} - \boldsymbol{x}'| \leq \kappa h$,

$$\mathrm{W}(\boldsymbol{x} - \boldsymbol{x}', h) = 0 \tag{5}$$

where *k* is the correlation constant with a smooth function at *X*

The standard expression of the kernel approximation is obtained as given by equation (6)

$$\langle f(\boldsymbol{x})\rangle = \int f(\boldsymbol{x}')W(\boldsymbol{x} - \boldsymbol{x}', h)\mathrm{d}\boldsymbol{x}' \approx \sum_{j=1}^{N} \frac{m_j}{\rho_j} f(\boldsymbol{x}_j)W(\boldsymbol{x} - \boldsymbol{x}'_j, h_i) \tag{6}$$

where m_j and ρ_j are the mass and density of particle *j*, respectively.

Particle approximation process[9]:

In another important calculation process (particle approximation), the particle in equation (6) can be approximated as follows:

$$\langle f(\boldsymbol{x})\rangle = \int f(\boldsymbol{x}')W(\boldsymbol{x} - \boldsymbol{x}', h)\mathrm{d}\boldsymbol{x}' \approx \sum_{j=1}^{N} \frac{m_j}{\rho_j} f(\boldsymbol{x}_j)W(\boldsymbol{x} - \boldsymbol{x}'_j, h_i) \tag{7}$$

Therefore,

$$\langle f(\boldsymbol{x}_{\mathrm{i}})\rangle = \sum_{j=1}^{N} \frac{m_j}{\rho_j} f(\boldsymbol{x}_j) W(\boldsymbol{x} - \boldsymbol{x}'_j, h_i) \quad (8)$$

where m_j is the mass of SPH particle *j*, and ρ_j is the density of particle j; therefore, $\frac{m_j}{\rho_j}$ is the volume associated with particle *j* or node *j*.

2.2 SPH equation of the jet and target

The Navier-Stokes equations of fluid media can be expressed by the conservation of mass,

$$\frac{d\rho}{dt} = -\rho \frac{\partial v^{\beta}}{\partial x^{\beta}} \quad (9)$$

The momentum conservation equation is expressed as follows:

$$\frac{dv^{\beta}}{dt} = \frac{1}{\rho} \frac{\partial \sigma^{\alpha\beta}}{\partial x^{\beta}} + f^{\alpha} \quad (10)$$

where ρ is the density of the fluid, *t* is the time, v^{β} is the velocity component, x^{β} is the position vector of the fluid, f^{α} is the external force, and α and β are Cartesian coordinates *x* and *y*, respectively. The repeated superscripts in the above equations conform to Einstein's summation rule.

In equation (11), $\sigma^{\alpha\beta}$ is the total stress tensor component, which consists,

$$\sigma^{\alpha\beta} = -p\delta^{\alpha\beta} + \tau^{\alpha\beta} \quad (11)$$

where $\delta^{\alpha\beta}$ is the Kronecker tensor (if $\alpha = \beta$, $\delta^{\alpha\beta}$= 1; otherwise, $\delta^{\alpha\beta}$=0)

In a Newtonian fluid, the viscous shear stress is directly proportional to the shear strain rate and is correlated by the proportional coefficient μ (viscosity coefficient).

$$\tau^{\alpha\beta} = \mu\varepsilon^{\alpha\beta} \quad (12)$$

where

$$\varepsilon^{\alpha\beta} = \frac{\partial v^{\beta}}{\partial x^{\alpha}} + \frac{\partial v^{\alpha}}{\partial x^{\beta}} - \frac{2}{3}(\nabla \cdot v)\delta^{\alpha\beta} \quad (13)$$

In the SPH approximation[10], the governing Navier-Stokes equations for the conservation of mass and momentum can be expressed as

$$\begin{cases} \frac{d\rho_i}{dt} = \rho_i \sum_{j=1}^{N} \frac{m_j}{\rho_j} v_{ij}^{\beta} \cdot \frac{\partial W_{ij}}{\partial x_i^{\beta}} \\ \frac{dv_i^{\alpha}}{dt} = -\sum_{j=1}^{N} m_j \frac{p_i + p_j}{\rho_i \rho_j} \frac{\partial W_{ij}}{\partial x_i^{\beta}} + \sum_{j=1}^{N} m_j \frac{\mu_i \varepsilon_i^{\alpha\beta} + \mu_j \varepsilon_j^{\alpha\beta}}{\rho_i \rho_j} \frac{\partial W_{ij}}{\partial x_i^{\beta}} \end{cases} \quad (14)$$

Artificial viscosity is added to the equation to represent the effect of a high-speed

water jet, so equation (14) can be transformed into the following equation[11]

$$\begin{cases} \frac{d\rho_i}{dt} = \rho_i \sum_{j=1}^{N} \frac{m_j}{\rho_j} v_{ij}^{\beta} \cdot \frac{\partial W_{ij}}{\partial x_i^{\beta}} \\ \frac{dv_i^{\alpha}}{dt} = -\sum_{j=1}^{N} m_j \left[\frac{p_i + p_j}{\rho_i \rho_j} - \frac{\mu_i \varepsilon_i^{\alpha\beta} + \mu_j \varepsilon_j^{\alpha\beta}}{\rho_i \rho_j} + \Pi_{ij} \right] \frac{\partial W_{ij}}{\partial x_i^{\beta}} \end{cases} \tag{15}$$

where Π_{ij} is the artificial viscosity. In this method, it is used to reduce the nonphysical oscillation in the numerical calculation process around impact area.

When the waterjet cuts the material, it is in a compression state, and the change in density produces pressure. The equation of state is in the Mie-Gruneisen form[12],

$$p = \frac{\rho_0 C^2 \mu [1 + \left(1 - \frac{\gamma_0}{2}\right)\mu - \frac{a}{2}\mu^2]}{[1 - (S_1 - 1)\mu - S_2 \frac{\mu^2}{\mu+1} - S_3 \frac{\mu^3}{(\mu+1)^2}]} + (\gamma_0 + a\mu)e \tag{16}$$

The material parameters and coefficients of the equation of state of the jet are shown in Table 1.

Table 1. Values of the water coefficient and parameters in the Mie-Gruneisen equation

Symbol	Parameter	Value
ρ_0	Initial density	1000 kg/m^3
C	Velocity of sound	1480 m/s
γ_0	Gruneisen gamma	0.5
a	Volume correction coefficient	0
S_1	Coefficient	2.56
S_2	Coefficient	1.986
S_3	Coefficient	1.2268

The SPH equation of the solid governing equation is[13]:

$$\begin{cases} \frac{d\rho_i}{dt} = \rho_i \sum_{j=1}^{N} \frac{m_j}{\rho_j} v_{ij}^{\beta} \cdot \frac{\partial W_{ij}}{\partial x_i^{\beta}} \\ \frac{dv_i^{\alpha}}{dt} = -\sum_{j=1}^{N} m_j \left[\frac{p_i + p_j}{\rho_i \rho_j} - \frac{\mu_i \varepsilon_i^{\alpha\beta} + \mu_j \varepsilon_j^{\alpha\beta}}{\rho_i \rho_j} + \Pi_{ij} \right] \frac{\partial W_{ij}}{\partial x_i^{\beta}} \end{cases} \tag{17}$$

In the numerical calculation of solid medium, the stress can be expressed as,

$$\sigma^{\alpha\beta} = -p\delta^{\alpha\beta} + S^{\alpha\beta} \tag{18}$$

The Jaumann rate is replaced by the stress deviator. The stress deviator can be expressed as,

$$\dot{S}^{\alpha\beta} = 2G\left(\dot{\varepsilon}^{\alpha\beta} - \frac{1}{3}\delta^{\alpha\beta}\dot{\varepsilon}^{\gamma\gamma}\right) + S^{\alpha\gamma}R^{\beta\gamma} + S^{\beta\gamma}R^{\alpha\gamma} \tag{19}$$

where G is the shear modulus and $\dot{\varepsilon}$ is the strain rate tensor, which can be expressed as

$$\dot{\varepsilon}^{\alpha\beta} = \frac{1}{2}\left(\frac{\partial v^{\alpha}}{\partial x^{\beta}} + \frac{\partial v^{\beta}}{\partial x^{\alpha}}\right) \tag{20}$$

$\dot{\varepsilon}^{\alpha\beta}$ is the rate of the rotation tensor, and

$$R^{\alpha\beta} = \frac{1}{2}\left(\frac{\partial v^{\alpha}}{\partial x^{\beta}} - \frac{\partial v^{\beta}}{\partial x^{\alpha}}\right) \tag{21}$$

(1) Constitutive model

The solid target is modeled as titanium alloy (TC4), and the constitutive model of the ductile material is the Johnson-Cook constitutive model[14],

$$\sigma_y = (A + B(\bar{\varepsilon}^p)^n)(1 + C\ln\dot{\varepsilon}_e^*)(1 - (T^*)^m) \tag{22}$$

$$\bar{\varepsilon}^p = \varepsilon^p/\varepsilon_0 \tag{23}$$

$$T^* = (T - T_r)/(T_m - T_r) \tag{24}$$

where σ_y is the stress yield of the material; A, B, C, m, and n are the relevant parameters of the material; $\bar{\varepsilon}^p$ is the equivalent plastic strain; $\dot{\varepsilon}_e^*$ is the dimensionless plastic strain rate; T^* is the homologous temperature; ε^p is the plastic strain; ε_0 is the reference strain rate; T is the actual temperature; T_r is room temperature; and T_m is the melting point of the material.

(2) Failure model

The Johnson-Cook fracture criterion[15] is adopted for the failure fracture behavior of the target material. The expression of loss effect change ε_f in the model is

$$\varepsilon_f = f(\sigma^*, T^*, \dot{\varepsilon}_e^*) = [D_1 + D_2 exp(D_3\sigma^*)][1 + D_4 ln\dot{\varepsilon}_e^*][1 + D_5 T^*] \tag{25}$$

$$\sigma^* = \frac{\sigma_m}{\sigma_{eq}} \tag{26}$$

where D_1, D_2, D_3, D_4 and D_5 are material performance parameters, σ_m is the average value of the main stress, and σ_{eq} is the equivalent stress.

(3) State equation

To calculate the isotropic pressure of the material, the Mie-Gruneisen equation is used to simulate the effect of the impact between high-speed abrasive particles and ductile materials. The equation of state can be expressed as

$$p = \frac{\rho_0 C_0^2 \eta\left(1+\left(1-\frac{\Gamma_0}{2}\right)\eta\right)}{(1-(S_a-1)\eta)} + \rho_0 \Gamma_0 e \tag{27}$$

where ρ_0 is the reference density (kg/m3); Γ_0 is the constant of the Gruneisen equation, S_a is the linear Hugoniot coefficient and E is the internal energy per unit mass. The specific parameters of TC4 are shown in Table 1

Table 1 Material parameters of Ti-6Al-4V

Parameter	Symbol	Numerical value
Density (kg/m^3)	ρ	4430
Elastic modulus (GPa)	E	110
Poisson's ratio	μ	0.33
Reference strain rate(s^{-1})	ε_0	4×10^{-4}
Room temperature (K)	T_r	293
Melting point (K)	T_m	1878
Johnson-Cook model parameters		
	A	1060 MPa
	B	1090 MPa
	C	0.0117
	n	0.884
	m	1.1
Johnson-Cook failure model parameters		
	D_1	-0.09
	D_2	0.27
	D_3	0.48
	D_4	0.014
	D_5	3.87

2.3 Movement of abrasive particles in water

The velocity of abrasive particles can be divided into the translation speed and rotation speed.

$$\begin{cases} \frac{dV_i^\alpha}{dt} = \frac{F_i^\alpha}{M_i} \\ \frac{dW_i^\alpha}{dt} = \frac{T_i^\alpha}{I_i} \\ \frac{dX_i^\alpha}{dt} = V_i^\alpha \end{cases} \tag{28}$$

where i is the ith abrasive particle, V_i^α and W_i^α are the translation speed and rotation speed, X_i^α is the position vector of the center of mass, M_i is the mass of the ith particle, I_i is the moment of inertia, F_i^α is the total force acting on the ith particle, and T_i^α is the total torque.

In this model, each particle is associated with a number of discrete SPH nodes, which carry the field variables including the mass and velocity. The equation of motion of the nodes is,

$$v_{j-i}^{\alpha} = V_i^{\alpha} + W_i^{\alpha} \times (x_{j-i}^{\alpha} - X_i^{\alpha}) \tag{29}$$

where j is the jth node and X_i^{α} is the position vector of the node.

2.4 Contact and fracture

In the process of impact, the jet is in contact with the target, and the target material is broken and fractured after being impacted. The contact and fixation between SPH particles is through the application of binding force. The radius of the support region of the SPH particles is twice as long as the smooth length. When the distance between two partices is twice the smooth length, the SPH particles will generate the corresponding contact force.

The contact potential function is defined as,

$$\phi(x_i) = \sum_j^{\mathrm{NCONT}} \frac{m_j}{\rho_j} K \left[\frac{W(r_{ij})}{W(\Delta d_{avg})}\right]^n \tag{30}$$

where NCONT is the number of particles belonging to different objects in the support domain of particle i, Δd_{avg} is the average distance of two SPH particles, and K and N are user-defined parameters. The value of K is related to the material properties and impact velocity.

After being extruded, the material will fracture when it exceeds the compression limit. The SPH method can predict the contact between the jet and the target and accurately describe the "contact" and "stripping" of the two components. During abrasive waterjet (AWJ) cutting, the target material will be removed by a high-speed AWJ. Therefore, the possibility of fracture must be considered in the SPH model. To simulate the fracture of the target material, the smooth length of the SPH particles at the fracture is reduced. This reduces the interaction between the fractured particles and other particles. However, reducing the smoothing length of invalid particles will lead to a decrease in the time step and an increase in the calculation time. Therefore, when a critical value is reached, the particle is considered invalid, and fracture is assumed to occur at the position related to the particle. Then, the particles on the site are removed

from the SPH calculation. However, to ensure the conservation of mass and momentum, the mass and momentum of invalid particles are still retained.

2.5 Artificial viscous force

In impact process, the artificial viscous force (artificial viscosity) is introduced into the solution method so that the algorithm can simulate the collision problem and eliminate any nonphysical oscillation. When the law of conservation of mass, momentum and energy is applied to the shock wave surface, kinetic energy is converted into heat energy. In the process of calculation, the energy is transformed into viscous dissipation. In this article, it can be expressed as[16]

$$\Pi_{ij} = \begin{cases} \frac{-\alpha_\Pi \bar{c}_{ij}\phi_{ij}+\beta_\Pi \phi_{ij}^2}{\bar{\rho}_{ij}} & , \boldsymbol{v}_{ij}\cdot\boldsymbol{x}_{ij}<0 \\ 0 & , \boldsymbol{v}_{ij}\cdot\boldsymbol{x}_{ij}\geq 0 \end{cases} \tag{31}$$

where α_Π and β_Π are the standard constants, and $\alpha_\Pi = 1$ and$\beta_\Pi = 1$

$$\phi_{ij} = \frac{h_{ij}\boldsymbol{v}_{ij}\cdot\boldsymbol{x}_{ij}}{|\boldsymbol{x}_{ij}|^2+\varphi^2} \tag{32}$$

$$\bar{c}_{ij} = \frac{1}{2}(c_i + c_j)$$

$$\bar{\rho}_{ij} = \frac{1}{2}(\rho_i + \rho_j)$$

$$h_{ij} = \frac{1}{2}(h_i + h_j)$$

$$\boldsymbol{v}_{ij} = \boldsymbol{v}_i + \boldsymbol{v}_j$$

$$\boldsymbol{x_{ij}} = \boldsymbol{x}_i + \boldsymbol{x}_j$$

In the above equation, *C* is the velocity of sound and *V* is the velocity vector related to the particle.

2.6 Time integration mode

The leap-frogging (LF) algorithm[17], which has the advantages of low memory requirements and high efficiency, is used in this artilce. When the calculation of a time step is completed, the density, velocity and internal energy advance a half step forward from the initial state, and the particle position advances by one step.

$$\rho_i^{\frac{1}{2}} = \rho_i^0 + \frac{\Delta t^1}{2}\frac{d\rho_i^0}{dt}$$

$$\boldsymbol{v}_i^{\frac{1}{2}} = \boldsymbol{v}_i^0 + \frac{\Delta t^1}{2}\frac{d\boldsymbol{v}_i^0}{dt}$$

$$\boldsymbol{x}_i^{\frac{1}{2}} = \boldsymbol{x}_i^0 + \frac{\Delta t^1}{2}\boldsymbol{v}_i^{\frac{1}{2}}$$

where Δt is the time step, ρ is the density of the particles, V is the velocity vector of particle motion, x is the position vector of the particles, and the upper corner of each parameter represents the time step.

In the overall calculation, to ensure that the parameters such as the density, velocity and internal energy of the particles can remain consistent with the position of the particles, the values of these parameters will advance half a time step forward at the beginning of each operation step to obtain the value of the integer step length.

$$\rho_{\mathrm{i}}^{\mathrm{n}} = \rho_{\mathrm{i}}^{\mathrm{n}-1/2} + \frac{\Delta t^{\mathrm{n}}}{2}\frac{\mathrm{d}\rho_{\mathrm{i}}^{\mathrm{n}-1}}{\mathrm{d}t}$$

$$v_{\mathrm{i}}^{\mathrm{n}} = v_{\mathrm{i}}^{\mathrm{n}-1/2} + \frac{\Delta t^{\mathrm{n}}}{2}\frac{\mathrm{d}v_{\mathrm{i}}^{\mathrm{n}-1}}{\mathrm{d}t}$$

where *n* represents the time step.

3. Modeling of an abrasive particle distribution based on a stochastic algorithm

Taking the modeling process of regular triangular abrasive particles as an example, a random distribution model of the angular particles is established in this paper. The characteristic parameters of abrasive particles include the particle shape and size, the incident angle and impact velocity, the reflection angle, the reflection velocity and the reflection angular velocity. As shown in Fig. 1, the incident velocity of the regular triangle particle is v_i, the angle between the incident velocity and the horizontal axis is the incident angle α_i, the reflection velocity of the abrasive particles after rebound is v_r, the angle between the reflection velocity and horizontal direction is reflection angle α_r, the reflection angular velocity is ω_r, the height of the equilateral triangle is h, and the contact angle of the angular particles is A. The length of the target material is l and the height is b.

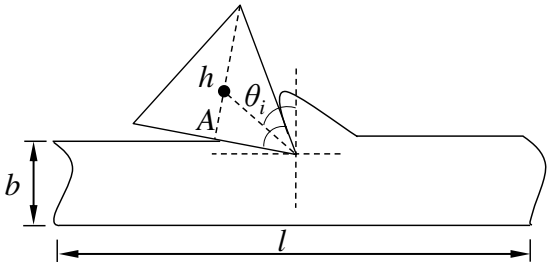

Fig. 1 Regular triangle particle impact diagram

In the actual abrasive water jet cutting process, the abrasive particles are randomly distributed in the water. A random algorithm is used to generate the abrasive particle distribution in the water, which replicates the working conditions. The initial angle of the abrasive particles is also random. Therefore, two random algorithms are used in this process. According to the initial water column width d_w, the distance between the water column and target l_w is the initial coordinate, as shown in Fig. 2. To simplify the distribution of abrasive particles during modeling, the particles in the jet are distributed in layers, such as the particle layers shown in the figure. The distribution of the particles in each particle layer is random. The number of layers of particles depends on the initial input value (such as the size of the abrasive particles).

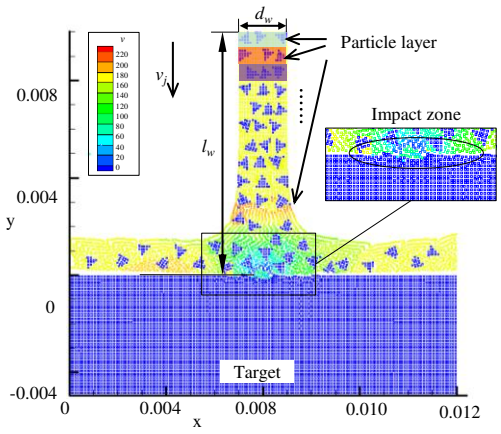

Fig. 2 Random distribution of abrasive particles

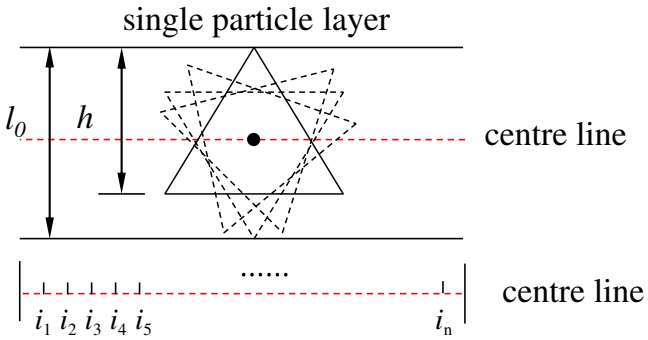

Fig. 3 Particle layer diagram

The maximum number of particles n_{max} can be obtained according to the geometric parameters of the abrasive particles and the jet size parameters. As shown in Fig. 3, the single particle layer spacing is l_o. When $l_o = \frac{3}{4}h$, the number of particle layers is the highest.

$$n_{max} = \frac{l_w}{\frac{4}{3}h}$$

The number of abrasive particles in each particle layer of the model is the same, assuming that the number of abrasive particles in each particle layer is *N*, the number of *N* abrasive particles from the left boundary to the right boundary is n_1, n_2, n_3, . . . , n_N, and the center point of the abrasive particles is located in the centerline of the particle layer. When the abrasive particles are randomly generated, the center coordinates of the abrasive particles are generated first. As shown in Fig. 3, the centerline of the particle layer is represented as the interval of [0,1], and the interval is divided into J (1), J (2), J (3), ,J(n).

$$J(i) = [Q_{i-1}, Q_i) \quad (i = 1,2 \cdots n)$$

$$Q_i = \sum_{k=1}^{i} q_k \qquad (i = 1,2 \cdots n), Q_0 = 0$$

According to the flow of the random algorithm, let $s = \lambda$, $\alpha_s = 0$, $\beta_s = 1$, and $I(s) = [\alpha_s, \beta_s]$, and a value a_r is randomly obtained from the input centerline sequence. Then, a subinterval of $I(s)$ is generated.

$$I(sa_r) = [\alpha_{sa}, \beta_{sa}]$$

$$\alpha_{sa} = \alpha_s + (\beta_s - \alpha_s)P_{a-1}$$

$$\beta_{sa} = \alpha_s + (\beta_s - \alpha_s)P_a$$

where $P_j = \sum_{k=1}^{j} p_k$, p_k is the probability distribution, and $P_0 = 0$. If $J(i)$ belongs to the generated subdomain $I(sa_r)$, the distance between the generated center point and the boundary of the left and right sides of the jet should be determined. For regular triangular abrasive particles, if $\Delta x_0 \geq \frac{2}{3}h$, the initial point can be generated, and its coordinates (x_1, y_1) can be stored. The above process is repeated until the *N*th central point (x_N, y_N) is generated, and the distance between the two points is determined.

$$\Delta x = \sqrt{x_N - x_{N-1}}$$

where x_N is the abscissa of the center point of the *N*th abrasive particle and (*N*-1) the abscissa of the (*N*-1)th abrasive particle. Since the center of the abrasive particle in each particle layer is located on the centerline, the influence of the ordinate can be ignored.

To ensure that there is no interference between the particles in the layer of particles, $\Delta x \geq \frac{4}{3}h$.

When generating the coordinates of the geometric points of abrasive particles, as shown in Fig. 4, assume that the coordinates of center point *A* of the abrasive particles are (x_0, y_0), and the impact angle of the particles is θ. According to the parameters previously assumed, *A* is the center point of the abrasive particles, and its coordinates are (x_0, y_0); then, the coordinates of the impact vertex of the equilateral triangle are (x_1, y_1)

$$\cos\theta_i = \frac{|x_1 - x_0|}{\frac{2}{3}h}$$

$$\sin\theta_i = \frac{y_0 - y_1}{\frac{2}{3}h}$$

Therefore,

$$x_1 = x_0 + \frac{2}{3}h \cdot \cos\theta_i$$

or

$$x_1 = x_0 - \frac{2}{3}h \cdot \cos\theta_i$$

$$y_1 = y_0 - \frac{2}{3}h \cdot \sin\theta_i$$

where x_1 is the abscissa value of the impact point and y_1 is the ordinate value of the impact point.

Therefore, the coordinates of the impact vertex of the triangular particles incident on the left side of the central axis are $a_1(x_0 + \frac{2}{3}h \cdot \cos\theta_i,\ y_0 - \frac{2}{3}h \cdot \sin\theta_i)$. The coordinates of particles incident on the right side of the central axis are $a_1(x_0 - \frac{2}{3}h \cdot \cos\theta,\ y_0 - \frac{2}{3}h \cdot \sin\theta)$. The other two vertices of the triangle are a_2 and a_3. The coordinate values are $a_2(x_2, y_2)$ and $a_3(x_3, y_3)$.

$$\cos(60° - \theta_i) = \frac{x_1 - x_2}{\frac{2\sqrt{3}}{3}h}$$

$$\sin(60° - \theta_i) = \frac{y_2 - y_1}{\frac{2\sqrt{3}}{3}h}$$

Therefore,

$$x_2 = x_1 - (\frac{\sqrt{3}}{3}\cos\theta_i + \sin\theta_i) \cdot h$$

$$y_2 = y_0 - （\frac{2+\sqrt{3}}{3}\sin\theta_i + \cos\theta_i） \cdot h$$

For vertex a_2,

$$\sin(\theta_i - 30°) = \frac{x_1 - x_3}{\frac{2\sqrt{3}}{3}h}$$

$$\cos(\theta_i - 30°) = \frac{y_3 - y_1}{\frac{2\sqrt{3}}{3}h}$$

Therefore,

$$x_3 = x_1 - (\sin\theta_i - \frac{\sqrt{3}}{3}\cos\theta_i) \cdot h$$

$$y_3 = y_0 + （\frac{\sqrt{3}-2}{3}\sin\theta_i + \cos\theta_i） \cdot h$$

Therefore, the coordinates of the other two vertices of the triangle abrasive particles are $a_2(x_2, y_2)$, $a_3(x_3, y_3)$, namely, $a_2(x_1 - (\frac{\sqrt{3}}{3}\cos\theta_i + \sin\theta_i) \cdot h,\ y_0 - （\frac{2+\sqrt{3}}{3}\sin\theta_i + \cos\theta_i） \cdot h)$, $a_3(x_1 - (\sin\theta_i - \frac{\sqrt{3}}{3}\cos\theta_i) \cdot h,\ y_0 + （\frac{\sqrt{3}-2}{3}\sin\theta_i + \cos\theta_i） \cdot h)$.

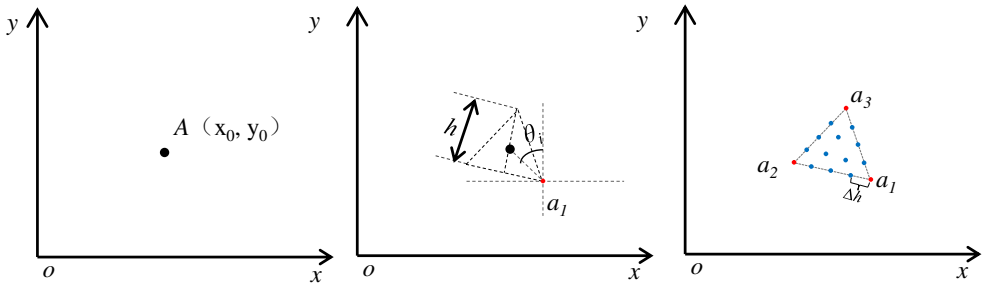

Fig. 4 Generation of abrasive particles with SPH particles

When generating SPH particles, a series of evenly distributed surface nodes are generated among the particles to determine the surface normal vector. As shown in Fig. 5, the surface normal vector of the node generated by the surface is

$$\vec{n}_{k+1} = \pm\left(\frac{y_{k+2} - y_k}{|\vec{x}_{k+2} - \vec{x}_k|}, -\frac{x_{k+2} - x_k}{|\vec{x}_{k+2} - \vec{x}_k|}\right)$$

where the nodes adjacent to k+1 are k and k + 2, and $\vec{x}_{k+2}$=(x_{k+2}, y_{k+2}) and $\vec{x}_k$=(x_k,

y_k).

Regular triangular particles can be triangulated when solving the moment of inertia of angular particles. After the triangulation of the diagonal particles, the coordinate of the center of mass is $\vec{x}_c$.

$$\vec{x}_c = \frac{\sum A_n \cdot \vec{x}_{nc}}{\sum A_n}$$

where A_n is the total area of angular particles and $\vec{x}_{nc}$ is the centroid coordinate of the subtriangle after subdivision.

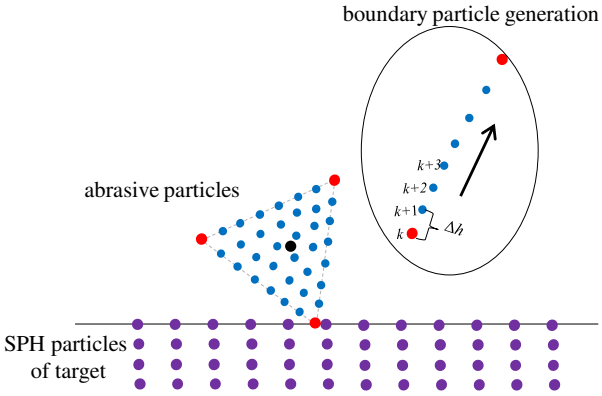

Fig. 5 Surface node diagram of the target particle and abrasive particles

Therefore, the mass and moment of inertia of the angular abrasive particles are as follows:

$$\begin{cases} M = \sum m_n \\ I_z = \sum (i_{zn} + m_n(\vec{x}_{nc} - \vec{x}_c)^2) \end{cases}$$

$$i_{zn} = \frac{m_n}{36}(a_n^2 + b_n^2 + c_n^2)$$

where I_z is the moment of inertia of the nth dissector triangle around its center of mass, m_n is the mass of the nth subtriangle, and the three sides of the subtriangle are a_n, b_n and c_n.

In a water jet column, the number of abrasive particles is also related to the initial abrasive concentration. In the initial setting, if the concentration of abrasive particles in the abrasive jet is set, the influence of the abrasive concentration on the generation of abrasive particles should be considered.

In the simulation of abrasive water jet cutting, the volume flow ratio of the abrasive particles to that of water is φ_m.

$$\varphi_m = \frac{V_p}{V_j} = \frac{V_p}{d_w \cdot l_w}$$

where V_p is the volume of abrasive particles distributed between the initial position of the jet and the target material and V_j is the volume of the jet.

V_{pe} is the volume of regular triangle particles, and it is expressed as the area in the 2D plane,

$$V_{pe} = \frac{\sqrt{3}h^2}{3}$$

where h is the height of an abrasive particle in the shape of an equilateral triangle, and a is the side length of an abrasive particle in the shape of a square.

Therefore, the volume flow ratio of the abrasive particles to that of water is

$$\varphi_m = \frac{V_p}{V_j} = \frac{\sqrt{3}h^2 N_{all}}{3d_w \cdot l_w}$$

where N_{all} is the total number of abrasive particles in the whole jet column.

The number of abrasive particles in the whole jet column can be determined based on the volume flow ratio of the abrasive particles and water. In the initial setting, if the concentration of abrasive particles needs to be considered, the two-dimensional abrasive water jet cutting model can be ensured to be the same as the actual cutting scenario. The flow chart of the random algorithm for the whole abrasive particle generation is shown in Fig. 6.

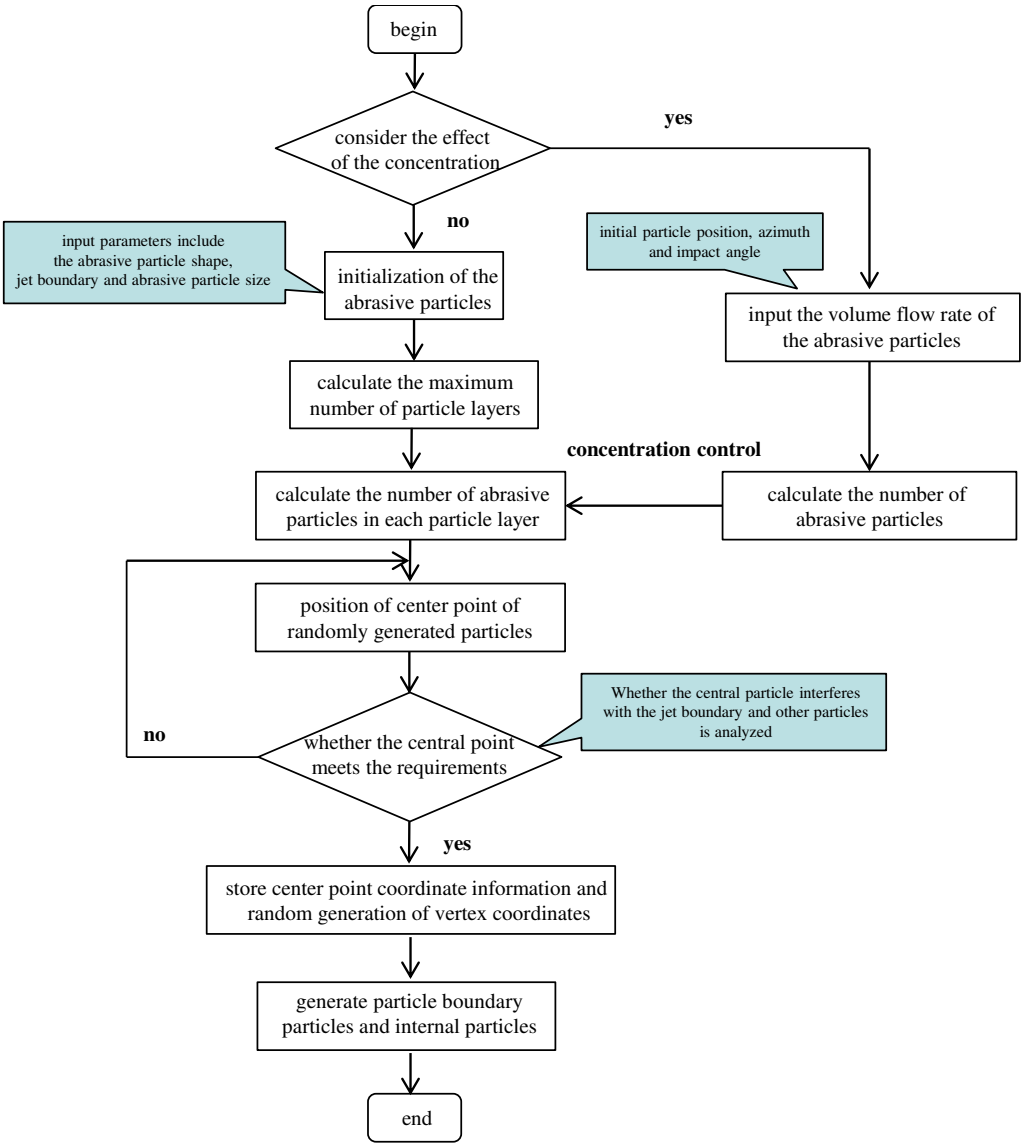

Fig. 6 Flow chart of the random algorithm

4. Simulations, numerical results and discussion

4.1 Simulation calculation

Taking two-dimensional triangular abrasive particles as an example, it is assumed that the abrasive particles are distributed along the centerline and the jet velocity (v_j) is 170 m/s. The cutting times of (a), (b), (c) and (d) in Fig. 6 are 0.2 s, 0.4 s, 1 s and 1.6 s, respectively. The corresponding cutting depths at different times are 0.15 mm, 0.32 mm, 1.20 mm and 2.00 mm. The target material is a ductile material.

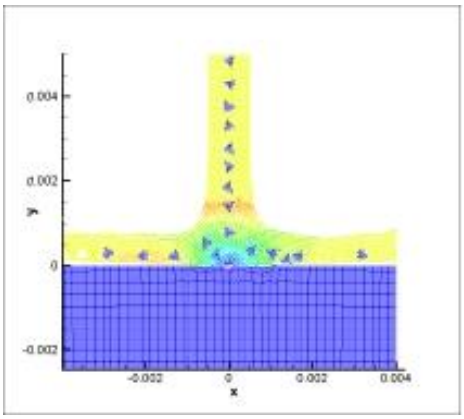

t=0.2 s

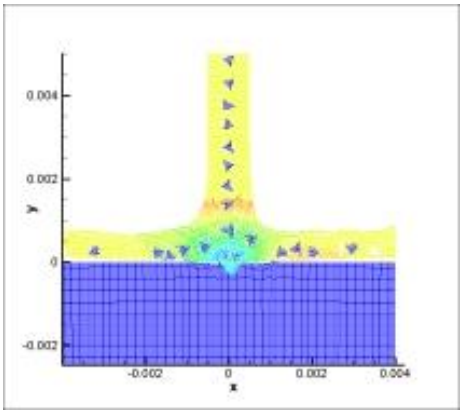

t=0.4 s

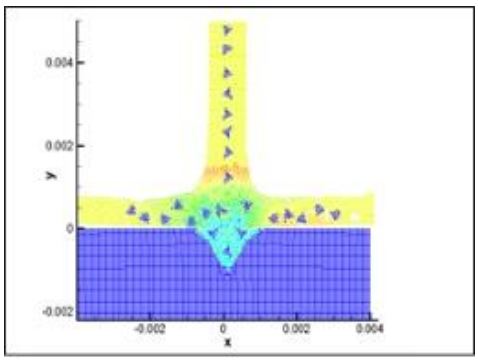

t=1.0 s

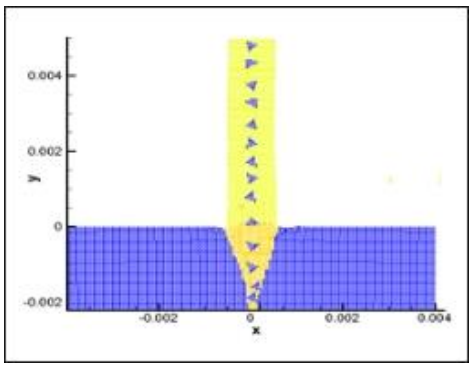

t=1.6 s

Fig. 7 Cutting process of a jet with a single row of abrasive particles

When the jet with a single row of abrasive particles impinges on the extended target, the notch in the center of the slit is obvious at the initial position, and the notch on both sides of the slit is shallow. With the deepening of the slit, the gap between the center and both sides increases. When the jet completely penetrates the target material, the slit presents a "V" shape.

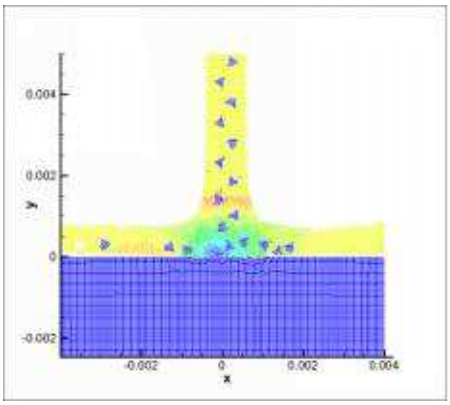

t=0.2 s

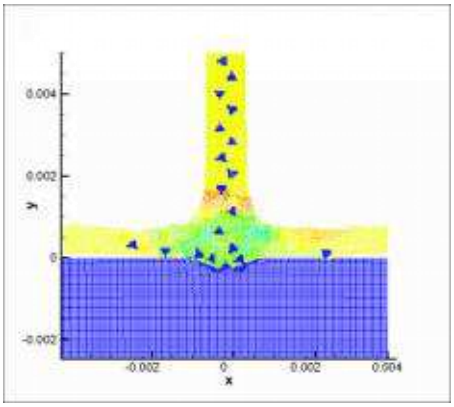

t=0.4 s

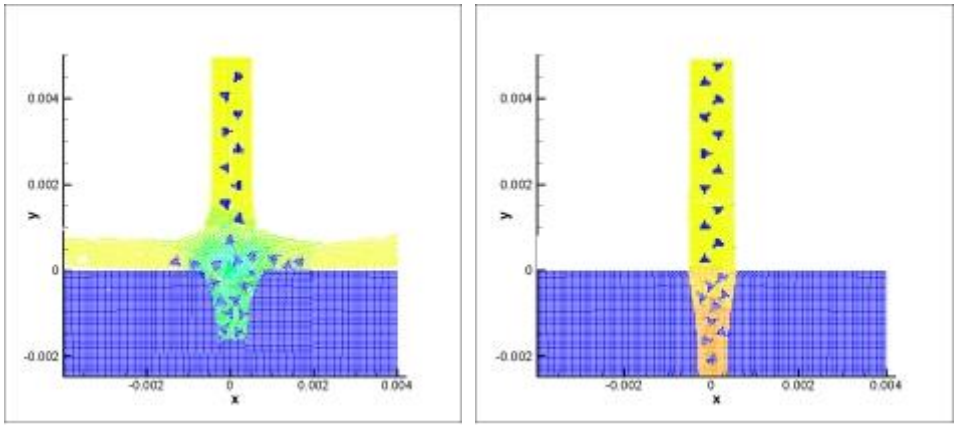

t=1.0 s t=1.6 s

Fig. 8 Cutting process of the jet with a double row of asymmetric abrasive particles

It is assumed that the abrasive particles are asymmetrically distributed along the centerline, the jet velocity v_j is 170 m/s, the cutting times are 0.2 s, 0.4 s, 1 s and 1.6 s, and the corresponding cutting depth at different times is 0.07 mm, 0.45 mm, 1.31 mm and 4.00 mm, respectively. The simulation results at different times are shown in Fig. 8. At the initial time, the notch is shallow, and the surface of the notch is uneven. When the target material is completely penetrated, the shape of the notch is similar to that of the single row of particles, but the slope is smaller than that of the single row of particles.

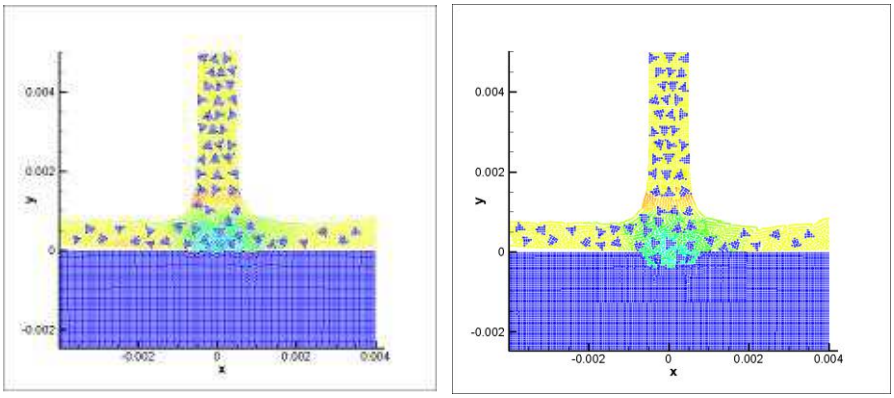

t=0.2 s t=0.4 s

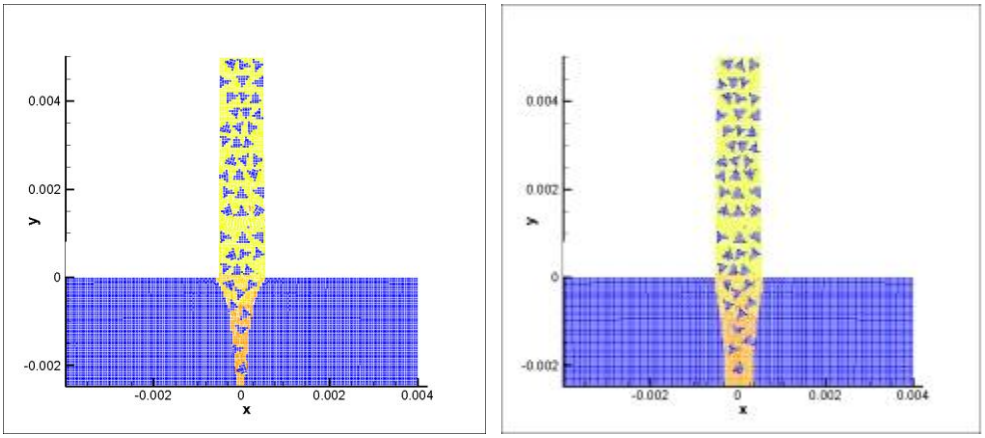

t=1.0 s t=1.6 s

Fig. 9 Cutting process of the abrasive jet with a random distribution

According to the actual volume ratio of abrasive particles, the abrasive particles are evenly arranged in the center of the jet, as shown in Fig. 10, and the time detection points are 0.2 s, 0.4 s, 1 s and 1.6 s. Compared with the simulation results using the random algorithm, the flatness of the dent at the initial time is higher than that of the surface formed by the jet with randomly distributed abrasives. The taper of the formed slit is smaller than that of the jet with a random distribution.

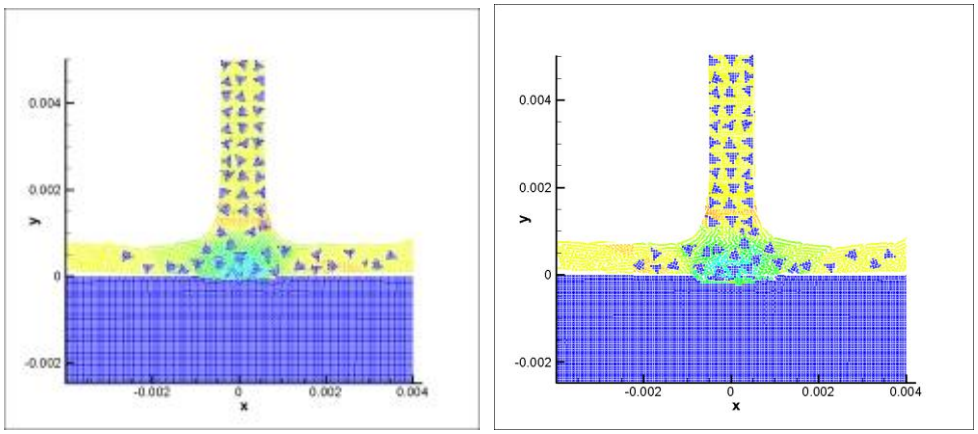

t=0.2 s t=0.4 s

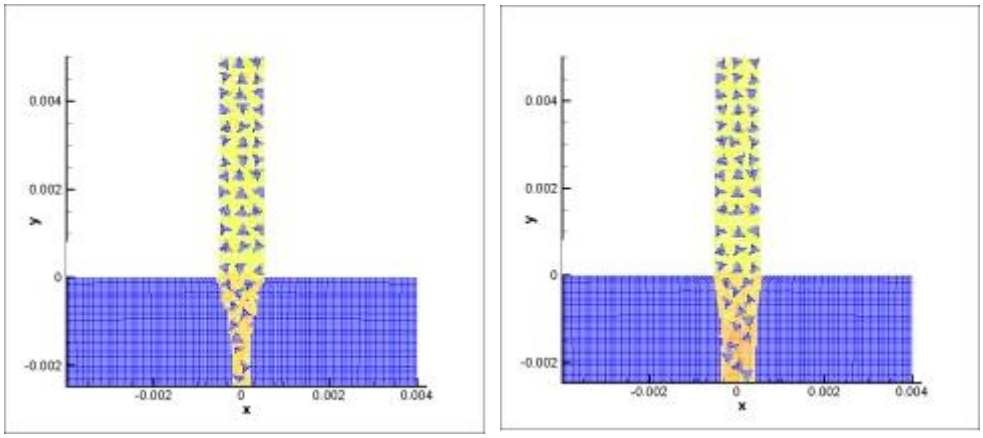

t=1.0 s t=1.6 s

Fig. 10 Cutting process of the abrasive jet with a uniform distribution

4.2 Comparison of the experimental results

The TC4 sample is cut with a jet velocity of 170 m/s as the initial condition. The jet cutting test bench is shown in Fig. 11, and the whole cutting dynamic process is captured by a high-speed camera. The comparison diagram of simulation results is shown in Fig. 12; the slit shapes formed by the jet cutting with randomly distributed particles and uniformly distributed particles are similar. Fig. 13 shows the shape of the cutting seam obtained after the actual cutting and the contour obtained by the point tracing method. The actual cutting thickness is 30 mm. After reducing the size of the cutting seam by ten times, the curve in Fig. 13 is obtained by comparing with the simulation results.

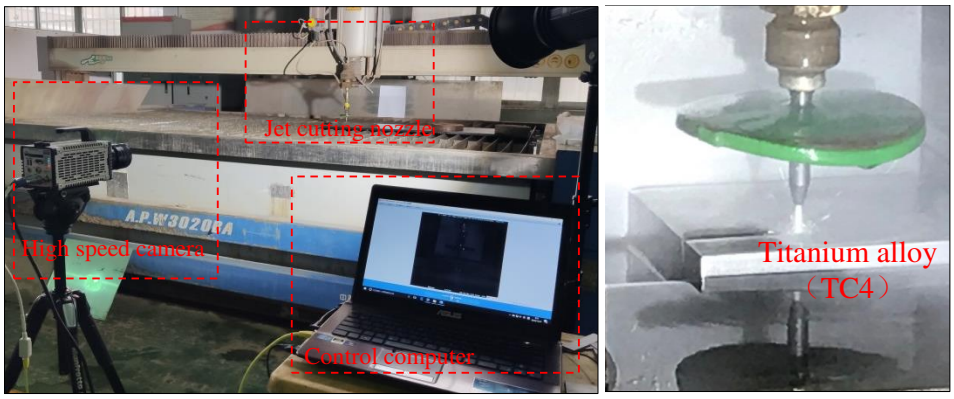

Fig. 11 Experimental drawing of abrasive waterjet cutting

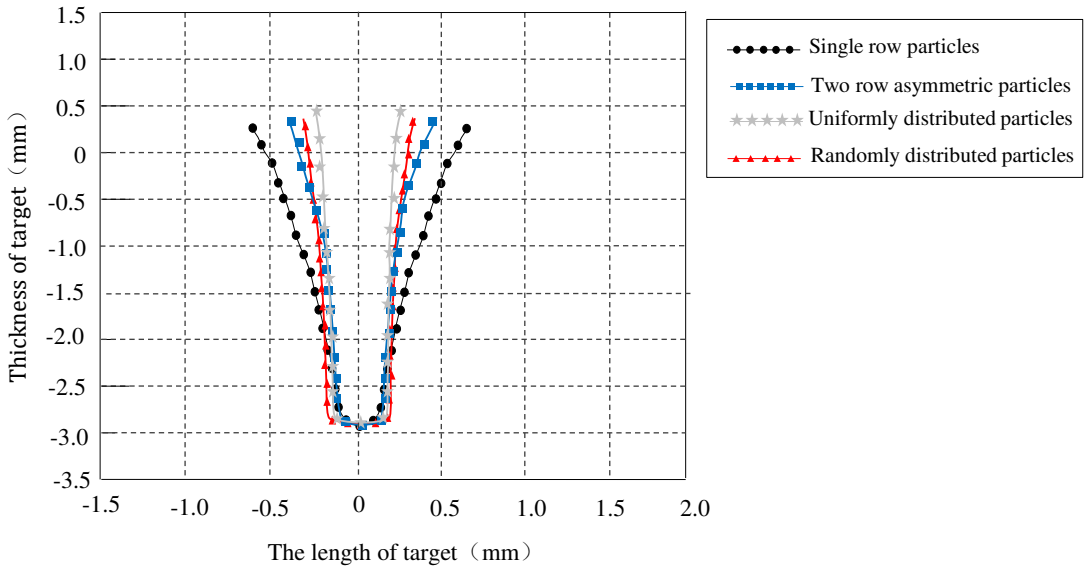

Fig. 12 Comparison diagram of the different cutting marks

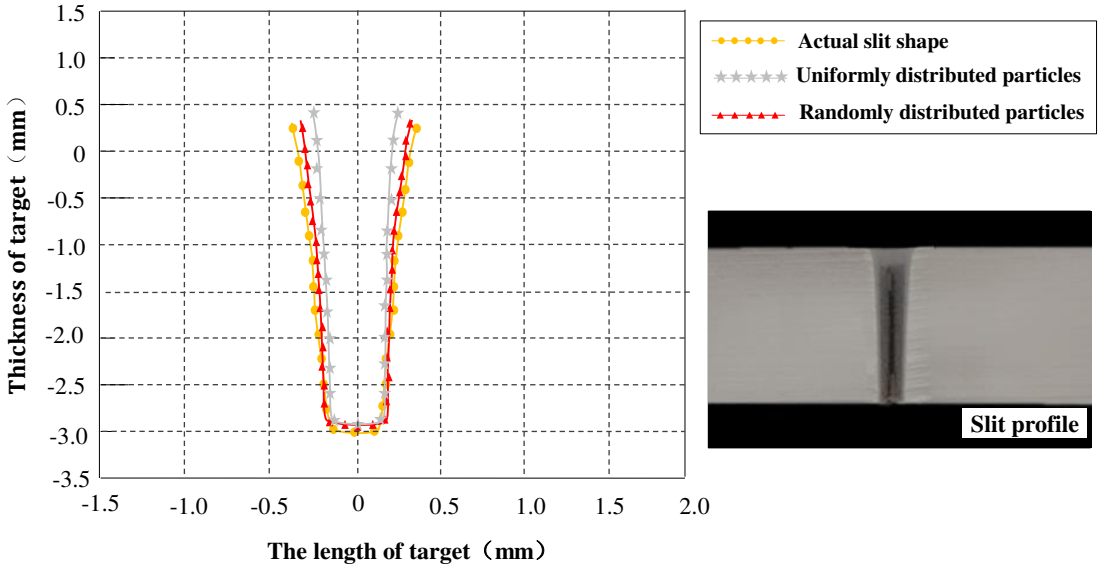

Fig. 13 Comparison of experimental results and simulation results

The results show that the slit shape formed by the jet with random abrasive particles is consistent with the actual cutting shape. A comparison of the dents formed by the jet on the surface at the initial time is shown in Fig. 14. The left side of the figure shows the dent formed on the material surface at the initial time of jet impact. A comparison between time dent and simulation results is also shown in Fig. 14. During the simulation, the extrusion accumulation of materials first occurs on both sides of the cutting area, and then a dent is formed, which is essentially consistent with the actual cutting process.

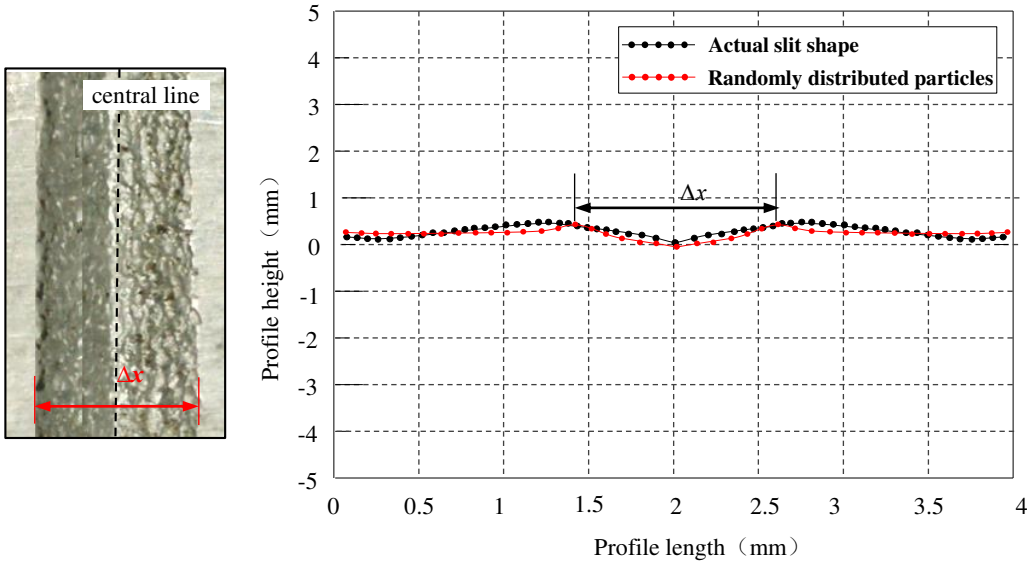

Fig. 14 Comparison of initial dent contours

4.3 Conclusion

This paper mainly studies the influence of the random distribution of abrasive particles on the numerical simulation of jet cutting. The SPH method is used in the modeling, and the random algorithm approach is incorporated to simulate the distribution of abrasive particles in water. Based on the results of numerical simulation and experimental study, the following conclusions are obtained

1. The influence of abrasive particle distribution on cutting was studied by using the SPH model. The numerical results show that the slot formed by the jet with random abrasive particles has a small taper and high parallelism.

2. Through the cutting of TC4 material, through the comparison between the experimental results and the simulation results, the numerical simulation results of the slit formed by the abrasive water jet with a random distribution match well with the experimental results. The model can well reflect the process of cutting the target material, and the random distribution model is suitably accurate in the study of the abrasive water jet cutting process.

Declarations section

a. Funding (information that explains whether and by whom the research was supported)

This research was funded by Shandong Provincial Natural Science Foundation, China, grant number: ZR2020QE164 and Qingdao applied research project funding.

b. Conflicts of interest/Competing interests (include appropriate disclosures)

The authors declared that they have no conflicts of interest to the article entitled "Modeling method and experimental study on the random distribution of abrasive particles in the jet cutting process". We declare that we do not have any commercial or associative interest that represents a conflict of interest in connection with the work submitted Authors: Long Feng, Qiang Zhang, Mingchao Du, Chunyong Fan, Kun Zhang.

c. Availability of data and material (data transparency)

All data generated or analysed during this study are included in this published article.

d. Code availability (software application or custom code)

The code used or analysed during the current study are available from the corresponding author on reasonable request.

e. Ethics approval (include appropriate approvals or waivers)

Not applicable

f. Consent to participate (include appropriate statements)

Written informed consent was obtained from all authors.

g. Consent for publication (include appropriate statements)

Availability of data and material

h. Authors' contributions (optional: please review the submission guidelines from the journal whether statements are mandatory)

Not applicable

References

[1] ElTobgy M S, Ng E, Elbestawi M A. Finite element modeling of erosive wear[J]. International Journal of Machine Tools and Manufacture, 2005, 45(11): 1337-1346.

[2] Babets K. Numerical modeling and optimization of waterjet based surface decontamination[D]. New Jersey Institute of Technology, 2001.

[3] Ahmed D H, Naser J, Deam R T. Particles impact characteristics on cutting surface during the abrasive water jet machining: Numerical study[J]. Journal of Materials Processing Technology, 2016, 232: 116-130.

[4] Feng L, Liu G R, Li Z, et al. Study on the effects of abrasive particle shape on the cutting performance of Ti-6Al-4V materials based on the SPH method[J]. The International Journal of Advanced Manufacturing Technology, 2019, 101(9-12): 3167-3182.

[5] Liang Z, Shan S, Liu X, et al. Fuzzy prediction of AWJ turbulence characteristics by using typical multi-phase flow models[J]. Engineering Applications of Computational Fluid Mechanics, 2017, 11(1): 225-257.

[6] Dong X, Li Z, Feng L, et al. Modeling, simulation, and analysis of the impact (s) of single angular-type particles on ductile surfaces using smoothed particle hydrodynamics[J]. Powder Technology, 2017, 318: 363-382.

[7] Liu, M. B., Liu, G. R., Lam, K. Y., et al. Smoothed particle hydrodynamics for numerical simulation of underwater explosion[J]. Computational Mechanics, 2003; 30(2): 106-118.

[8] Feng L, Dong X, Li Z, et al. Modeling of Waterjet Abrasion in Mining Processes Based on the Smoothed Particle Hydrodynamics (SPH) Method[J]. International Journal of Computational Methods, 2020, 17(09): 1950075.

[9] Monaco A D, Manenti S, Gallati M, et al. SPH modeling of solid boundaries through a semi-analytic approach[J]. Engineering Applications of Computational Fluid Mechanics, 2011, 5(1): 1-15.

[10] G. R. Liu, M. B. Liu. Smoothed particle hydrodynamics: a meshfree particle method[M]. World Scientific, 2003.

[11] Jianming W, Na G, Wenjun G. Abrasive waterjet machining simulation by SPH

method[J]. The International Journal of Advanced Manufacturing Technology, 2010, 50(1-4): 227-234.

[12] Shyue K M. A fluid-mixture type algorithm for compressible multicomponent flow with Mie–Grüneisen equation of state[J]. Journal of Computational Physics, 2001, 171(2), 678-707.

[13] Pu JH, Shao S, Huang Y , et al. Evaluations of SWEs and SPH Numerical Modeling Techniques for Dam Break Flows[J]. Engineering Applications of Computational Fluid Mechanics, 2013, 7(4): 544-563.

[14] Johnson F R, Cook W H. Fracture characteristics of three metals subjected to various strains, strain rates, temperatures and pressures[J]. Engineering fracture mechanics,1985, 21(1), 31-48.

[15] Dai Zhou, Si Chen, Lei Li, Huafeng Li & Yaojun Zhao. Accuracy Improvement of Smoothed Particle Hydrodynamics[J]. Engineering Applications of Computational Fluid Mechanics,2008, 2:2, 244-251.

[16] Monaghan J. J., Gingold R. A. Shock simulation by the particle method SPH[J]. Journal of Computational Physics, 52: 374-389.

[17] Bui H H, Sako K, Fukagawa R. Numerical simulation of soil–water interaction using smoothed particle hydrodynamics (SPH) method[J]. Journal of Terramechanics, 2007, 44(5): 339-346.